

AD _____

Award Number: DAMD17-02-1-0664

TITLE: Analysis of Keratin Filament Assembly/Disassembly and Structure Following Modification by Sulfur Mustard Analogs

PRINCIPAL INVESTIGATOR: John F. Hess, Ph.D.

CONTRACTING ORGANIZATION: University of California at Davis
Davis, California 95616

REPORT DATE: July 2003

TYPE OF REPORT: Annual

PREPARED FOR: U.S. Army Medical Research and Materiel Command
Fort Detrick, Maryland 21702-5012

DISTRIBUTION STATEMENT: Approved for Public Release;
Distribution Unlimited

The views, opinions and/or findings contained in this report are those of the author(s) and should not be construed as an official Department of the Army position, policy or decision unless so designated by other documentation.

20031212 114

REPORT DOCUMENTATION PAGE

Form Approved
OMB No. 074-0188

Public reporting burden for this collection of information is estimated to average 1 hour per response, including the time for reviewing instructions, searching existing data sources, gathering and maintaining the data needed, and completing and reviewing this collection of information. Send comments regarding this burden estimate or any other aspect of this collection of information, including suggestions for reducing this burden to Washington Headquarters Services, Directorate for Information Operations and Reports, 1215 Jefferson Davis Highway, Suite 1204, Arlington, VA 22202-4302, and to the Office of Management and Budget, Paperwork Reduction Project (0704-0188), Washington, DC 20503

1. AGENCY USE ONLY (Leave blank)			2. REPORT DATE July 2003	3. REPORT TYPE AND DATES COVERED Annual (15 Jun 2002 - 14 Jun 2003)
4. TITLE AND SUBTITLE Analysis of Keratin Filament Assembly/Disassembly and Structure Following Modification by Sulfur Mustard Analogs			5. FUNDING NUMBERS DAMD17-02-1-0664	
6. AUTHOR(S) John F. Hess, Ph.D.				
7. PERFORMING ORGANIZATION NAME(S) AND ADDRESS(ES) University of California at Davis Davis, California 95616 E-Mail: jfhess@ucdavis.edu			8. PERFORMING ORGANIZATION REPORT NUMBER	
9. SPONSORING / MONITORING AGENCY NAME(S) AND ADDRESS(ES) U.S. Army Medical Research and Materiel Command Fort Detrick, Maryland 21702-5012			10. SPONSORING / MONITORING AGENCY REPORT NUMBER	
11. SUPPLEMENTARY NOTES Original contains color plates: All DTIC reproductions will be in black and white.				
12a. DISTRIBUTION / AVAILABILITY STATEMENT Approved for Public Release; Distribution Unlimited				12b. DISTRIBUTION CODE
13. ABSTRACT (Maximum 200 Words) Characterization of vimentin intermediate filament (IF) structure by site directed spin labeling (SDSL) and electron paramagnetic resonance (EPR) has produced new data concerning the A11 arrangement of molecules in intact filaments. In the A11 alignment, rod 1B of a dimer is aligned with rod 1B of a second dimer. Our EPR data identify vimentin position 190 as the midpoint of overlap between dimers in the A11 arrangement. In conjunction with previously published data, we have thus identified contact surfaces between individual amino acids of rod 1B and rod 2B, involved in assembly of IFs. Analysis of keratin filament assembly and disassembly following treatment with the vesicant analogs 2-chloroethyl ethyl sulfide (CEES) and mechlorethamine (MEC) has been performed with 2 keratin pairs, one bacterially produced and one isolated from bovine tissue. Experiments with bacterially produced keratin 8 and 18 show that Intermediate Filaments assembled <i>in vitro</i> and subsequently treated with CEES and MEC are severely altered. The normal filament network is destroyed, replaced by aggregates of material with an irregular appearance. Experiments with k5 and k14 isolated from bovine tissue reveal the same results; CEES and MEC treatment destroy the smooth filamentous appearance of normal IFs and result in large aggregates.				
14. SUBJECT TERMS No Subject Terms Provided.				15. NUMBER OF PAGES 24
				16. PRICE CODE
17. SECURITY CLASSIFICATION OF REPORT Unclassified	18. SECURITY CLASSIFICATION OF THIS PAGE Unclassified	19. SECURITY CLASSIFICATION OF ABSTRACT Unclassified	20. LIMITATION OF ABSTRACT Unlimited	

NSN 7540-01-280-5500

Standard Form 298 (Rev. 2-89)
 Prescribed by ANSI Std. Z39-18
 298-102

Table of Contents

Cover.....	1
SF 298.....	2
Table of Contents.....	3
Introduction.....	4
Body.....	5
Key Research Accomplishments.....	10
Reportable Outcomes.....	10
Conclusions.....	10
References.....	12
Appendices.....	13

Introduction

Vesicant induced skin blistering can be compared to inherited skin blistering diseases by the skin blistering phenotype. Inherited skin blistering diseases are generally the result of mutations in intermediate filament (IF) genes coding for any one of several pairs expressed in the skin. Unfortunately, the site or site of action of vesicants is unknown. It has been hypothesized that intermediate filaments (IFs) in the basal and suprabasal layers of the skin are damaged by vesicants and that the vesicant induced damage to the cytoskeleton results in skin blistering, a process mechanistically different, yet phenotypically similar to inherited skin blistering diseases. The goal of the research supported by this award is the characterization of vesicant modification of keratin IFs and keratin proteins and the effects of these modifications on keratin structure, assembly and disassembly.

As proposed in the approved statement of work, the analysis of keratin filament assembly and disassembly will be performed using techniques that we originally adapted to the study of vimentin assembly. Vimentin is a homopolymeric intermediate filament protein and thus is very similar, yet simpler than keratin intermediate filament assembly, which is heteropolymeric. Our initial results have been published (appendix 1), and additional results on the characterization of vimentin assembly are described below.

The second part of the body of this report focuses on the treatment of 2 different keratin filament networks with analogs of the skin blistering chemical weapon mustard gas (sulfur mustard, dichlorodioethyl sulfide). As originally proposed in the statement of work, a cysteine specific modification reagent would be employed to model protein modification by sulfur mustard. However, US Army personnel conducted a site visit in July of 2002 and pointed out more typical analogs of sulfur mustard commonly used in vitro. Therefore, the studies described below use the agents 2 chloroethyl ethyl sulfide (CEES) and mechlorethamine (MEC) as analogs of sulfur mustard.

Analysis of Vimentin IFs by EPR

Analysis of the effects of vesicants on the structure of keratin intermediate filaments (KIFs) is hampered by both the lack of a defined structure for intact KIFs and the lack of a method to study keratin assembly intermediates following vesicant exposure. As documented in the original proposal and published (1) (appendix 1), we have pioneered the use of site directed spin labeling (SDSL) and electron paramagnetic resonance (EPR) to determine IF structure. This method of IF structure determination provides a method to analyze filament assembly intermediates and assembled filaments. Our model system for the validation of SDSL-EPR to the study of IF structure is the homopolymeric IF protein vimentin.

In our original proposal, we presented data that demonstrated the ability of SDSL to identify alpha helical coiled coil structure, measure distances between labeled positions in both intact filaments and assembly intermediates, and finally, study interactions between assembly intermediates. We were able to show that the alpha helical coiled coil pattern, predicted to dominate the central region of all intermediate filaments, was easily recognized by EPR spectroscopy. From this characterization, we were able to resolve a discrepancy in the literature as to whether vimentin positions 305-312 were alpha helical rod domain 2B or part of a non-helical linker region (2, 3). Spectroscopy specifically identified vimentin positions 305-312 as alpha helical. In addition, this alpha helical heptad repeat pattern is in phase with the heptad repeat pattern from 316-337 (1).

Using the same technique, we were able to show that labels positioned on the exterior of the helix could be used to identify specific molecular arrangements. Thus, crosslinking experiments had produced data that were interpreted as an antiparallel alignment of vimentin molecules with rods 2B adjacent (termed the A22 alignment). Several crosslinks were identified, supporting a general structure. We proceeded to place spin labels on the exterior of the alpha helix and determined that position 348 was either the midpoint or very close to the midpoint of the overlap between rods 2B. We then predicted that several helical turns downstream and upstream of 348 we would find additional interactions. We were able to show that positions 334 and 359 were located on apposing surfaces of vimentin dimers in "protofilaments" and intact filaments.

With data in hand to characterize the A22 vimentin dimer alignment, we began constructing a series of mutants to use the same SDSL-EPR strategy to identify positions at apposing faces of dimers in the A11. Only one crosslink in vimentin rod 1B was identified by Steinert et al. as being consistent with the A11 alignment: lysine 187 crosslinked with itself (4). Examination of the sequence of rod 1B as presented by Conway and Parry (2), revealed the prediction that amino acids 170-200 should be located entirely within rod 1B and should be entirely alpha helical coiled coil. From the heptad repeat pattern, we chose several positions to individually introduce cysteine amino acids for spin labeling (see figure 1).

Construction of the individual mutants was performed in a cassette wise fashion using a Xho I-Cla I fragment as a template. Oligonucleotides containing the desired codon change were used with the Stratagene Quik Change kit; mutants were sequenced and the mutant cassette subcloned back into an expression vector. Individual mutant proteins were produced by bacterial expression and purified as described (1). Figure 1 shows normalized EPR spectra from three mutants, revealing alpha helical structure throughout this region with positions 171 and 175 (predicted to be an "a/d" heptad positions) consistent with this prediction. EPR spectra of mutant 176 shows the taller, less broadened character of non-a/d positions.

This simple result, the identification that this region of rod 1B is alpha helical, is actually quite important, as individual regions of IF proteins are *hypothesized* to be alpha helical, but the actual demonstration that a particular region is in fact alpha helical has only been performed recently by **x-ray crystallography of IF fragments**. Thus, part of rod 2B and part of rod 1A have been crystallized and shown to be alpha helical; rod 2B was in a coiled coil configuration but rod 1A was not!

EPR spectra were recorded from multiple mutants in the 170-193 region at various assembly stages. From these room temperature spectra, evidence for spin-spin interaction could be seen as broadening and flattening of the curve. Thus, from room temperature spectra of samples in low ionic strength buffers or samples in filament assembly buffer, we could select a few for further examination at low temperature.

Table 1

Position	d1/d values
187(f)	0.42*
188(g)	0.39
189(a)	0.47
190(b)	0.48*
193(e)	0.38
186(e)+193(e)	0.41*
187(f)+193(e)	0.43*
188(g)+193(e)	0.50*

*spins interact

To measure distances between spin labels positioned on the outside of the helix, we assembled both single labeled samples and mixtures of samples into filaments or protofilaments and collected spectra from frozen samples. From the frozen spectra, d1/d ratios were calculated, revealing the distance between spin labels within the filament. Figure 3B in our JBC paper (appendix 1) shows a graph of d1/d ratios plotted for 14 positions within rod 2B of vimentin. The plot reveals the dichotomy between heptad positions that are located at the a/d positions and those at non-a/d positions. Results obtained from rod 1B conform to the same pattern: the d1/d value calculated for a position 189 is 0.47; the value for non a/d position 193 is 0.38. The d1/d values for positions in this region are presented in table 1.

The non-a/d samples 187 and 190 showed d1/d values that were atypical. Using our background data as a reference, we conclude that spin-spin interaction between dimers is responsible for these high

d1/d values. Also, based on our previous experience, we expect that samples 191 and 192 will not show such strong evidence of spin-spin interaction due to the alpha helical coil of each peptide chain moving the spin labels farther apart. Mixtures of singly labeled proteins were also subject to filament assembly followed by collection of low temperature spectra collection and calculation of d1/d ratios. Thus, the d1/d ratio increases as mutants 186, 187 and 188 are mixed with spin labeled 193. **These data both confirm the interaction between dimers at this region of rod 1B and identify the interaction as an anti-parallel interaction.** An additional double mutant is presently in preparation to test these conclusions: vimentin 184C and 197C should produce spin-spin interactions, further identifying surfaces of rod 1B apposed to each other.

These data are consistent with the A11 alignment identified by crosslink data published by Steinert et al. (5). Our spectroscopy data published in JBC (appendix 1) identified the A22 alignment leaving one significant overlap left to document by EPR: the anti-parallel A12 alignment. The A11 alignment (described here) and A22 alignment (described in appendix 1) are staggered, and intellectually seem to fit together in such a way as to form a "protofilament"; furthermore, the stagger provides a structural basis for elongation of a growing IF (6). To

complement this simple view, the A12 alignment is the surface on the backside of each staggered A11 or A22 arrangements, uniting individual protofilament strands. Steinert et al have identified crosslinks within K5 and K14 KIFs and vimentin IFs that support such an alignment (4, 5). Based on crosslinks identified between vimentin molecules supporting the A12 alignment, we created a series of mutants between position 169 and 181 to examine by EPR. These mutants were selected due to the possibility that existing mutants in the 330-340 region would interact with 170-180. This preliminary approach was not definitive. No single mixture of samples provided clear evidence of interaction. Therefore, additional mutants will be created to look for a midpoint of overlap, analogous to experiments used to demonstrate the A11 and A22 alignments. Following the completion of these experiments, predictions can be made about residues in proximity in the A12 alignment in the regions we have already studied.

Analysis of Keratin Filament proteins

The approved *Statement of Work* proposed the creation of expression clones for human keratin k5 and k14 that contained coding sequences optimized for bacterial expression. Such constructs were hypothesized to increase the generally low levels of bacterial keratin 5/14 expression. A bacterial codon optimized K14 sequence was obtained from Bionexus, Oakland, CA; preliminary experiments do not reveal a dramatic increase in bacterial expression, which is unexpected. A number of new *E. coli* strains have been introduced in the past few years and these may produce higher levels of expression; such experiments have not been performed. It is also possible that expression of K14 will be higher if its assembly partner K5 is expressed in the same bacterial cell. This has not been tested, but will be. At the same time that codon optimized expression constructs were being synthesized, mutants were to be created such that endogenous cysteine codons were replaced by serine. K14 cysteines 367 and 389 have been individually replaced by serine and are additionally being combined; thus, 3 separate mutants are being produced: k14 ser367 cys389, k14 cys367 ser389 and k14 ser367 ser389. K14 cysteines 5 and 40 will be created using a PCR based approach with mutagenic oligonucleotides (see figure 2). By virtue of the locations of amino and carboxy terminal cysteines, clones can be recombined by restriction enzyme digestion and subcloning, eliminating the need to perform multiple mutagenesis reactions in a sequential process.

The codon optimized sequence of K5 is currently being assembled from individual subunits. Each subunit was created by assembling overlapping oligonucleotide primers in a PCR based procedure. Each subunit ends with a recognition sequence for a restriction enzyme. Thus, each subunit can be isolated as a restriction fragment that can be ligated to the next fragment, ultimately creating the full length construct. At the present time, 7 fragments of 2-300 bp, representing the complete K5 cDNA sequence have been made and their sequences determined to be correct (see figure 2). The amino terminal fragments 1-5 have been ligated together into a single construct. The last 2 fragments of the coding sequence are cloned together and will then be linked to the amino terminal 5 to create the entire coding sequence.

Creation of cysteine minus K5 clones is following right behind creation of the full length expression construct. Of the 7 different restriction fragments being assembled and cloned to form the K5 sequence, 4 contain a single cysteine codon. Thus, each individual clone containing a cysteine codon was used as a template in a Quik-change mutagenesis reaction (Stratagene, La Jolla, CA). Each cysteine codon has been changed to a serine codon and the change verified by

DNA sequencing. Each clone can be individually inserted into the expression construct by restriction enzyme digestion and ligation of the mutant fragment into the construct.

As a precursor to the proposed experiments and as a direct result of information provided during the site visit in 2002 by US Army representatives, I have performed the following experiments demonstrating the damage that vesicant related chemicals can cause to IF proteins: treatment of keratin filaments with 2 chloroethyl ethyl sulfide (CEES) or mechlorethamine (MEC) followed by examination of filament integrity in the electron microscope or treatment of keratin proteins with CEES or MEC followed by dialysis to assemble filaments and then examination in the electron microscope. Results in each case have been similar: **the vesicants CEES and MEC induce dramatic changes to established IF networks and render urea soluble keratin proteins filament assembly incompetent.**

Initial experiments were performed using bacterially expressed vimentin, either wild type or a cysteine minus mutant that has been shown to be filament assembly competent. IFs formed by either of these proteins were severely damaged by treatment with CEES. However, these experiments will not be discussed further. They are important for subsequent generalizations and will be included in planned publications.

The initial experiments performed with keratins utilized purified bacterially expressed human k8 and k18. K8/18 are expressed in early embryonic ectoderm and in adult undifferentiated epithelia. In vitro, we have assembled k8/18 keratin intermediate filaments (kIFs) using several assembly procedures. We have adopted the following as a standard method. Dialysis of mixtures of keratins at 0.2mg/ml for 2 hours in 8M urea, 10 mM Tris, pH 7.5, 1 mM DTT; 2 hours of dialysis at 4M urea, with 10 mM tris, pH 7.5, 1 mM DTT; 2 hours of dialysis against 10 mM tris pH 7.5, 1mM DTT and finally, overnight dialysis against 10 mM tris pH 7.5, 50 mM NaCl, 1mM MgCl₂, 1mM DTT. Samples are harvested and an aliquot prepared for electron microscopy. The remainder is divided into several tubes for treatment as follows: 1) DMSO (or 100% ethanol) solvent control, 2) 10mM CEES 3) 10mM MEC.

Figure 3 shows representative views of electron microscope fields from samples as labeled. Control filaments are, as expected, long smooth filaments with some bundling of filaments into larger diameter structures. Such structures are common and normal (7). Treatment of filaments with DMSO seems to have a slight effect; this has not been quantified, and is in no way comparable to treatment with 10mM CEES or MEC. The DMSO treated and control filaments each exhibit areas of high protein concentration and consequently, regions of over staining. The DMSO treated filaments show extended long smooth filaments as seen in the control.

The lower half of figure 3 however shows complete destruction of the IF networks. Both the 10 mM CEES and 10 mM MEC have modified the filaments and resulted in the extreme aggregation of proteins into large blobs. Within the blobs, regions of large diameter rope like structure are evident, but it is extremely rare to find a single place where a normal IF remains. Comparison of CEES and MEC treated samples reveals subtle differences. The CEES samples seem to cause more aggregation, with less evidence of filamentous connections between amorphous precipitates. MEC seems to result in aggregation with higher level aggregation at places, resulting an intensely staining "bead".

Figure 4 shows a typical experiment designed to identify the time course and chemical sensitivity of filaments to CEES. Using a final concentration of CEES of 1 mM, IFs seem swollen. Two different microscope fields are presented; each shows regions of apparently normal filaments with the presence of larger diameter filaments. The last panel shows again the

destruction of filaments that is produced by 10 mM CEES. Longer incubation times with 1 mM CEES do not produce dramatic evidence of changes to the filament network. Preliminary results show that 2 and 4 hours times look similar with perhaps more destruction in 6 hour (data not shown). The influence of extended times and DTT in the filament assembly buffer needs to be further investigated and will be. Similar experiments with MEC at 1 mM show similar results. Additional experiments are planned to fully characterize effects of MEC on IF networks.

Figure 5 shows the effects of CEES and MEC on bovine k5/14 filaments. The control sample shows normal looking filaments (as well as very small crystals of uranyl acetate, the white dots). Treatment of the sample with CEES and MEC results in exactly the same damage as seen with k8/18. At 10 mM concentrations, filaments are non-existent, in their place are aggregates of material. At 1 mM concentrations, both CEES and MEC have less obvious effects: slight aggregation and slight unraveling of filaments.

These data indicate the injurious effects of CEES and MEC on IFs, and thus support the hypothesis that modification of IFs *in vivo* could be responsible for the observed skin blistering effects of vesicants.

Key Research Accomplishments

- created series of site specific cysteine mutants localized to rod 1B of human vimentin.
- using SDSL-EPR, identified the A11 alignment of dimers in a vimentin IF
- demonstrated the alpha helical coiled coil structure of amino acids 171-193.
- determined that treatment of vimentin IFs with 2-chloroethyl ethyl sulfide (CEES) or mechloramine (MEC) results in massive aggregation and destruction of normal IFs
- determined that treatment of k8/18 IFs with CEES or MEC results in massive aggregation and destruction of normal IFs
- determined that treatment of k8/18 protein monomers in 8M urea with CEES or MEC prevents filament assembly.
- determined that treatment of k5/14 IFs with CEES or MEC results in massive aggregation and destruction of normal IFs.

Reportable Outcomes

Research presented in this annual report will be the subject of at least 2 manuscripts.

First, SDSL-EPR has been able to identify a molecular arrangement of proteins within a vimentin IF that was hypothesized by crosslink data. Our data provide a direct validation of proposed IF structural models and provide a framework for additional experiments to map apposing surface between vimentin dimers in the A11 structure. In addition, our method allows for the study of vimentin structure at different stages of assembly. Thus, in contrast to all other techniques used to study IF assembly, we are in a position to identify the structure of tetramers formed in either low ionic strength or low urea concentration buffers. Such data will illuminate the order of assembly of vimentin subunits, which should be similar to the assembly of other classes of IFs.

Secondly, our data are the first to show that treatment of keratin proteins and keratin filaments with analogs of skin blistering chemical weapons is able to destroy filament networks and render keratin proteins unable to assemble into filaments. These data are thus consistent with the hypothesis that skin blistering following vesicant exposure is due to damage to intermediate filament networks, followed by collapse of the filament network and ultimately, lysis of epithelial cells, leading to the blistering. Furthermore, the actions of these chemical weapons analogs (CEES and MEC) are the same using the homopolymeric IF protein vimentin.

Conclusions

The research described in this report clearly supports the ongoing investigation of the relationship between IF proteins and vesicants. Our in vitro data unequivocally show that *less*

potent analogs of vesicant chemical weapons are able to destroy assembled IF networks at relatively low concentrations. Furthermore, the same analogs are able to modify IF proteins such that they are unable to assemble.

Continued investigation of the IF/vesicant relationship will be facilitated by the SDSL-EPR approach we have pioneered. Our previous data identified a method to identify the A22 alignment of dimers and we have recently collected data that identify the A11 alignment. The last major alignment to be investigated is A12.

References

1. J. F. Hess, J. C. Voss, P. G. FitzGerald, *Journal of Biological Chemistry* **277**, 35516-22 (Sep 20, 2002).
2. J. F. Conway, D. A. D. Parry, *Int. J. Biol. macromol.* **10**, 79-98 (1988).
3. K. Albers, E. Fuchs, *International Review of Cytology* **134**, 243-79 (1992).
4. P. M. Steinert, L. N. Marekov, D. A. Parry, *Biochemistry* **32**, 10046-56 (1993).
5. P. M. Steinert, L. N. Marekov, D. A. Parry, *Journal of Biological Chemistry* **268**, 24916-25 (1993).
6. D. A. Parry, L. N. Marekov, P. M. Steinert, *Journal of Biological Chemistry* **276**, 39253-8 (Oct 19, 2001).
7. S. Yamada, D. Wirtz, P. A. Coulombe, *Mol Biol Cell* **13**, 382-91 (Jan, 2002).

Central Rod Domain

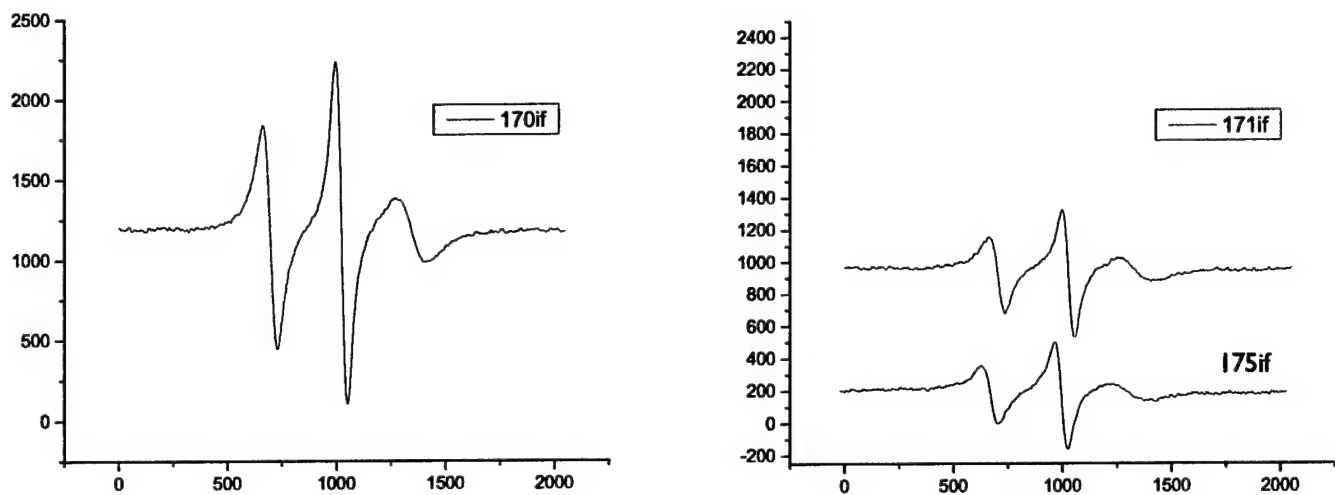
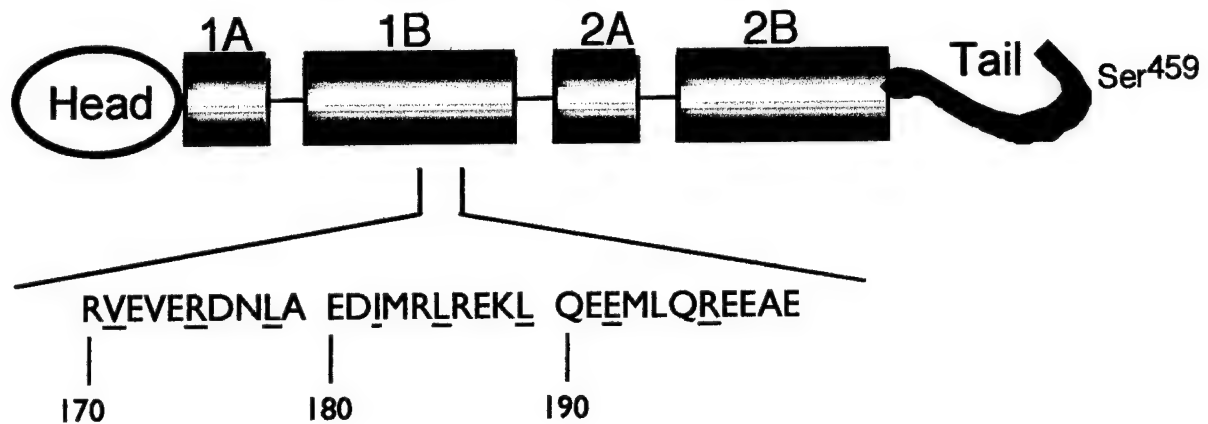
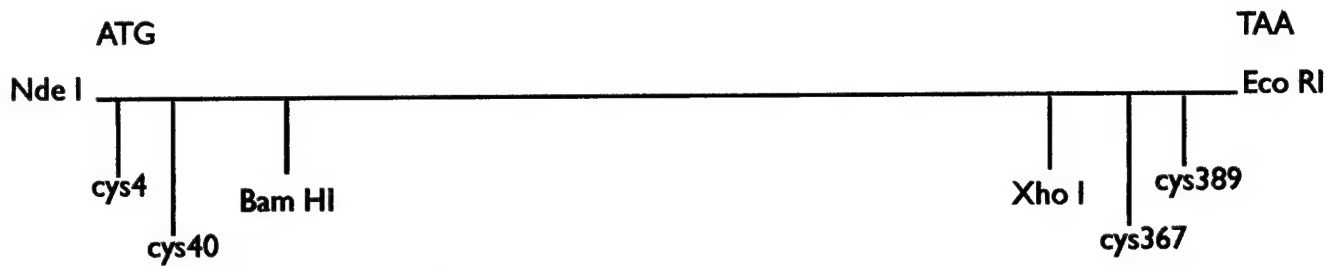


Figure 1, Vimentin structure and EPR of rod 1B

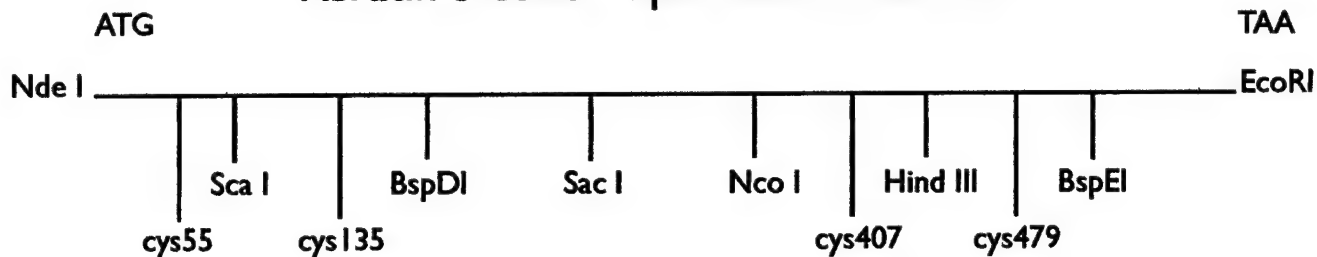
Keratin 14 codon optimized construct



clones constructed:

- full length Nde-RI in pCR Blunt
- full length Nde-RI in pT-7 for bacterial expression
- amino terminal region as a Bam HI fragment into pBKS II
- carboxy terminal region as Xho I fragment into pBKS II
- carboxy terminal region, ser 367 in pBKS II
- carboxy terminal region ser 389 in pBKS II

Keratin 5 codon optimized construct



clones constructed:

- the following fragments have been cloned into pCR 2.1
- Nde-Sca, Sca-BspDI, BspDI-SacI, SacI-Ncol, Ncol-HindIII, HindIII-EcoRI

Mutants have been constructed:

Nde-Sca ser 55, Sca-BspDI ser 135, Ncol-HindIII ser 407, HindIII-BspEI ser 479

fragments assembled in preparation for assembly:

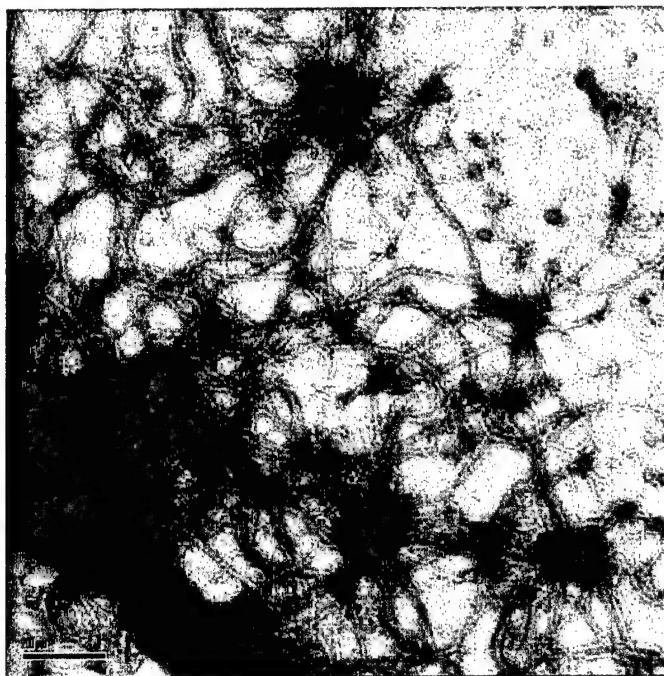
in pACT2J- NdeI-BspDI and NdeI-SacI

in pBKSII Sac-HindIII and HindIII- RI

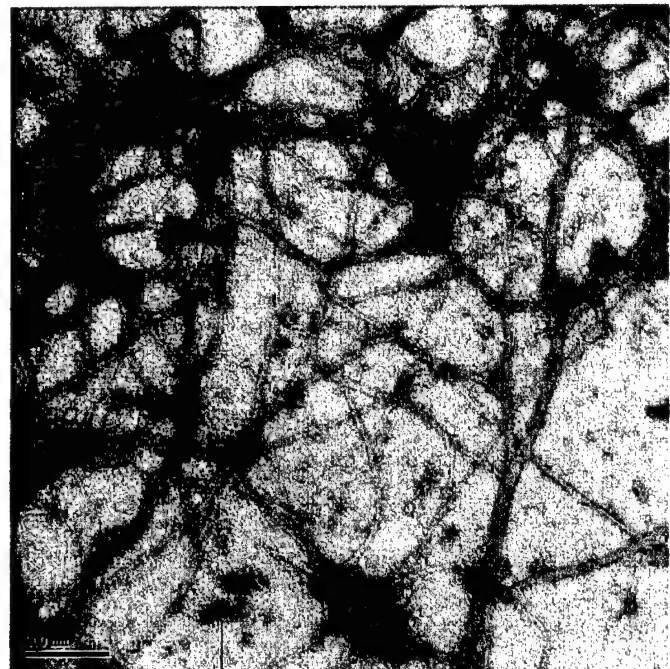
in pT7, Nde-HindIII

Figure 3 keratin 5/14 constructs and clones

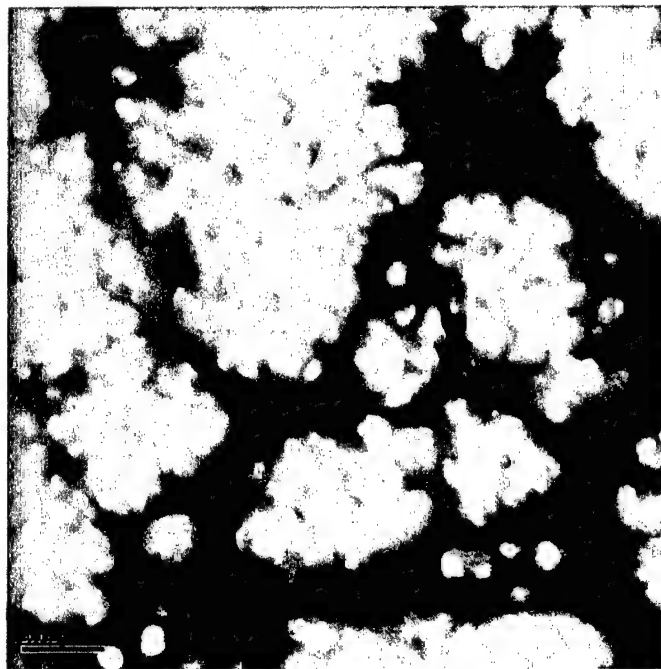
Figure 3, K8/18 filaments altered by CEES and MEC



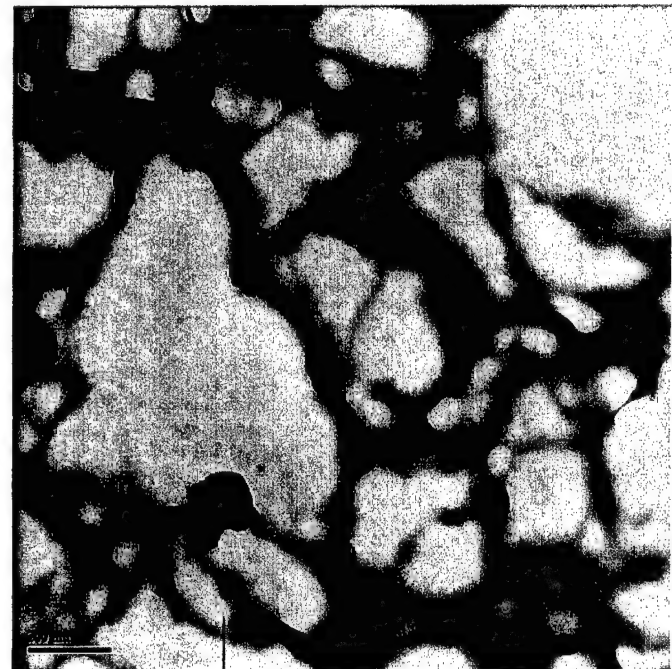
Control K8/18 filaments



K8/18 filaments, DMSO solvent control

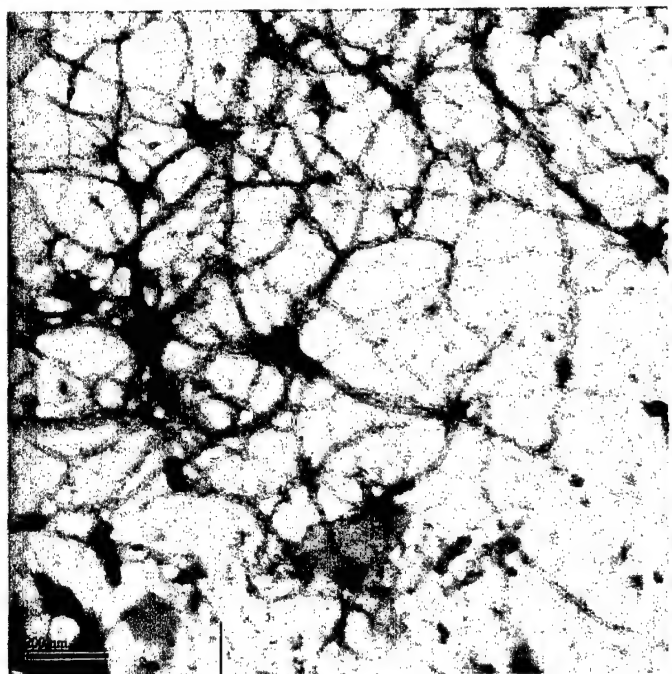


K8/18 filaments, 10mM CEES

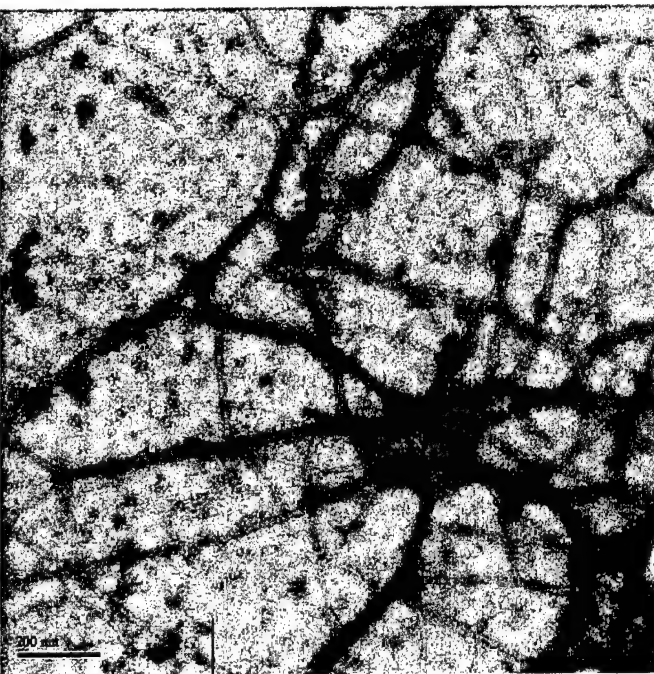


K8/18 filaments, 10mM MEC

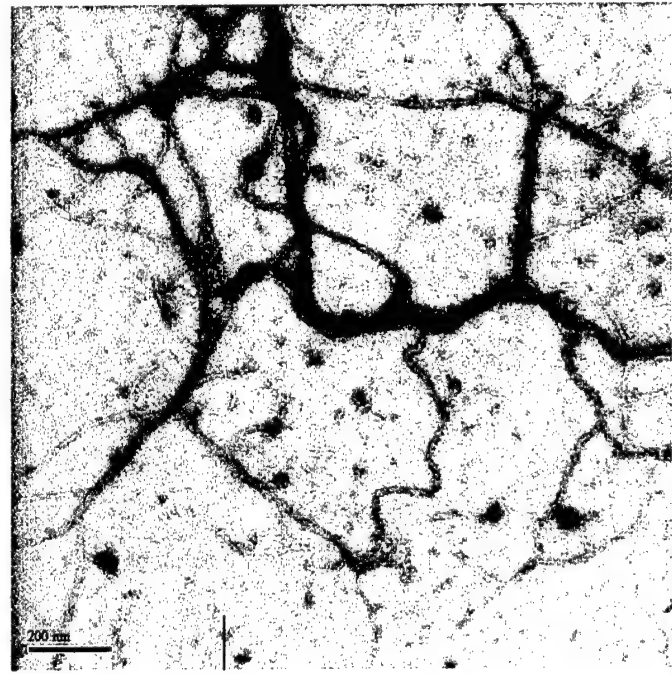
Figure 4, CEES treated K8/18 filaments



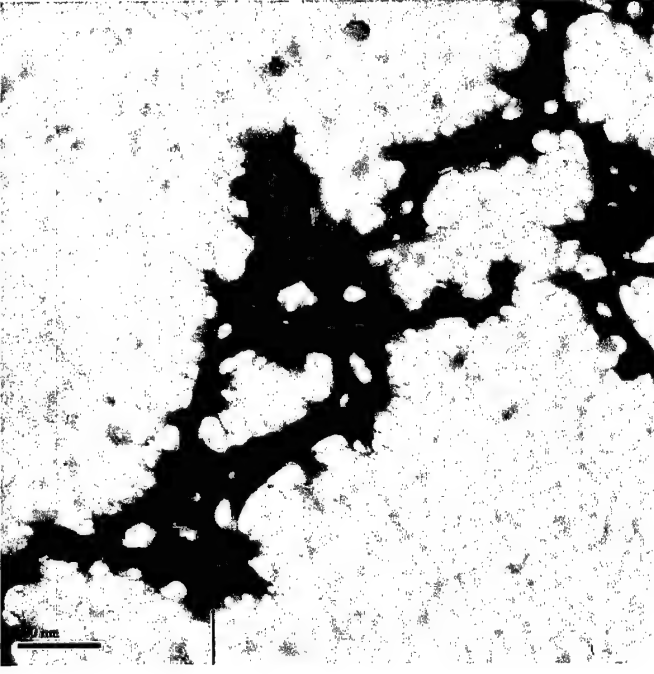
control (untreated)



1 mM CEES 2 hours



1 mM CEES, 2 hour

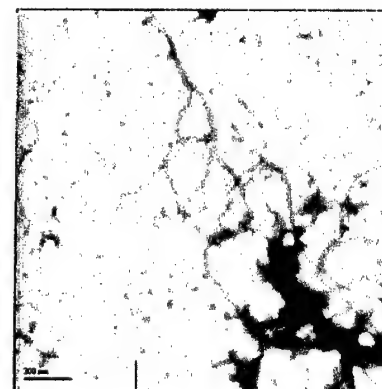


10 mM CEES, 2 hour

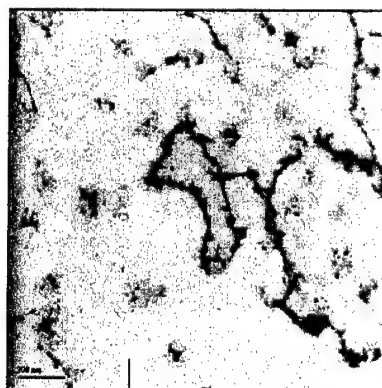
Figure 5, bovine k5/14 treated



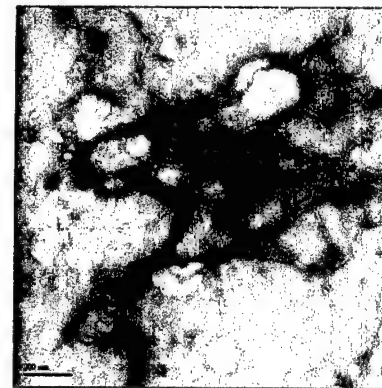
control (untreated)



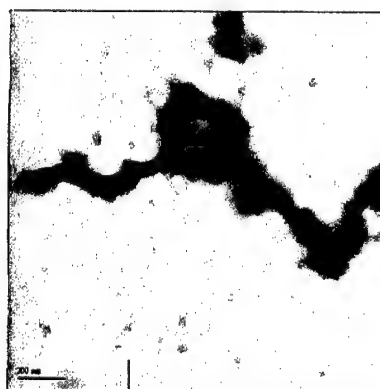
1 % DMSO



1 mM CEES



1 mM MEC



10 mM CEES



10 mM MEC

Real-time Observation of Coiled-coil Domains and Subunit Assembly in Intermediate Filaments*

Received for publication, July 1, 2002

Published, JBC Papers in Press, July 16, 2002, DOI 10.1074/jbc.M206500200

John F. Hess‡, John C. Voss§, and Paul G. Fitzgerald†¶

From the ‡Department of Cell Biology and Human Anatomy and the §Department of Biological Chemistry, University of California, School of Medicine, Davis, California 95616

We have utilized electron paramagnetic resonance spectroscopy to study secondary structure, subunit interaction, and molecular orientation of vimentin molecules within intact intermediate filaments and assembly intermediates. Spectroscopy data prove α -helical coiled-coil structures at individual amino acids 316–336 located in rod 2B. Analysis of positions 305, 309, and 312 identify this region as conforming to the helical pattern identified within 316–336 and thus demonstrates that, contrary to some previous predictions, this region is in an α -helical conformation. We show that by varying the position of the spin label, we can identify both intra- and inter-dimer interactions. With a label attached to the outside of the α -helix, we have been able to measure interactions between positions 348 of separate dimers as they align together in intact filaments, identifying the exact point of overlap. By mixing different spin-labeled proteins, we demonstrate that the interaction at position 348 is the result of an anti-parallel arrangement of dimers. This approach provides high resolution structural information (<2 nm resolution), can be used to identify molecular arrangements between subunits in an intact intermediate filament, and should be applicable to other noncrystallizable filamentous systems as well as to the study of protein fibrils.

Several human diseases have been traced to point mutations in human IF¹ genes (1–5). However, the mechanism(s) by which mutations produce disease has not been elucidated because the crystal structure has not been solved for any IF protein (6), although partial sequences have been solved (7, 8). Primary sequence analysis suggests that all IF proteins have a central rod domain composed principally of what is predicted to be an α -helical sequence flanked by variably sized head and tail domains (Fig. 1 shows a schematic of the IF protein vimentin) (9–11). In rare instances, the tail may be absent (12, 13). The central rod domain is relatively uniform in size (about 310 amino acids) and format, consisting of four coil domains separated by three short linker domains (14–16). The former are mainly characterized by a primary sequence containing a heptad repeat pattern (designated as residues *a*–*g*), a signature for

an α -helical coiled-coil dimer (17, 18). In this motif, the *a* and *d* positions are usually occupied by hydrophobic side chains, which promote the coiled association between two parallel α -helices. Circular dichroism studies of IFs confirm the presence of substantial levels of α -helical content, but without a solved crystal structure the exact identification of α -helical and non-helical regions within the central rod domain is imprecise.

Extensive cross-linking studies have been conducted to determine the arrangement of proteins in IFs (19, 20). Although data have been generated that are consistent with the initial formation of an in-parallel and in-register dimer and the subsequent assembly of these dimers, the interpretation of such data is not always straightforward and must be made cautiously. For example, cross-links between Cys³²⁸ of vimentin have been interpreted as occurring between chains within a dimer (intra-dimer), as well as between chains of separate dimers (inter-dimer) (21, 22).

These same issues, protein solubility and the inability to achieve crystallization, have plagued efforts to illuminate the molecular structure and interactions of membrane proteins. However, discrete structural information of membrane protein architecture has been achieved through site-directed spin labeling (SDSL) and electron paramagnetic resonance (EPR). We report here the use of these techniques to ask specific questions about the architecture of IF proteins and the arrangement of proteins within IFs.

Generally, SDSL is performed by engineering a unique cysteine amino acid into the peptide chain at a chosen position and modifying the free sulfhydryl with a thiol-specific nitroxide spin label. Subsequent EPR spectra of the spin-labeled side chain can be interpreted to provide information relevant to the relationship of protein structure and function (23, 24). Side chain dynamics measured from the EPR line shape data reflect backbone and contact-limited motions, information used to elucidate local secondary structure as well as protein folding and assembly (25). Furthermore, the interaction between site-directed spin labels is used to determine spatial relationships in proteins, information required to solve structure at the tertiary and quaternary levels. Because of its sensitivity and capability for real-time measurements under physiological conditions, EPR spectroscopy is particularly attractive for investigating conformational dynamics and mapping protein associations (24).

The ocular lens is composed of a large central mass of fiber cells expressing the IF proteins vimentin, filensin, and phakinin (CP49) surrounded by a single layer of lens epithelial cells expressing the IF protein vimentin (26). Vimentin is homopolymeric, whereas filensin and CP49 are copolymers. A mouse vimentin knockout displayed no obvious phenotype, but mutations in the fiber cell-specific protein CP49 can cause cataracts in humans (27–29). As a precursor to the

* This work was supported by National Institutes of Health Grant RO1EY08747 and Core Grant P30EY-12576 (both to P. G. F.) and by a UC Davis Health Sciences Research Fund grant (to J. F. H.). The costs of publication of this article were defrayed in part by the payment of page charges. This article must therefore be hereby marked "advertisement" in accordance with 18 U.S.C. Section 1734 solely to indicate this fact.

† To whom correspondence should be addressed. Tel.: 539-752-7130; Fax: 530-752-8520; E-mail: pgfitzgerald@ucdavis.edu.

‡ The abbreviations used are: IF, intermediate filament; SDSL, site direct spin labeling; EPR, electron paramagnetic resonance; SDS, sodium dodecyl sulfate; PAGE, polyacrylamide gel electrophoresis.

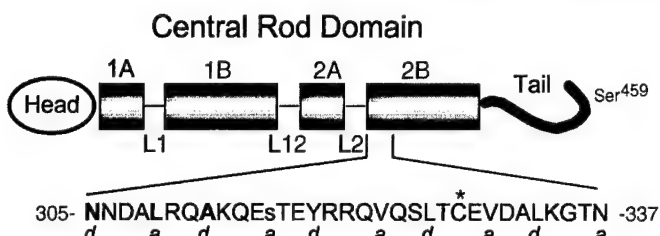


FIG. 1. Vimentin schematic. The predicted vimentin molecule is shown diagrammatically, with the central rod domain emphasized. α -helical rod subdomains 1A, 1B, 2A, and 2B are shown as shaded boxes. Hypothesized non-helical linker regions L1, L12, and L2 are drawn as thin lines. The region of rod subdomain 2B subject to study is expanded, and the sequence of this region is shown in single-letter amino acid abbreviations. Positions 305, 309, and 312 are bold; position 316 is lowercase. An asterisk marks the site of the single endogenous cysteine. Letters *a* and *d* below the amino acid sequence represent positions within individual heptad repeats in this area. The location of Ser⁴⁵⁹ is abstractly indicated near the end of the vimentin tail.

analysis of CP49 and filensin structure and assembly, we performed experiments with the homopolymeric IF protein vimentin as a model system. This report documents the utility of an SDS-EPR-based approach to study IF assembly, documenting α -helical coiled-coil structures at individual amino acids and identifying arrangements of molecules within an intact filament.

MATERIALS AND METHODS

Vimentin was produced by bacterial expression using pET vectors and isopropyl- β -D-thiogalactopyranoside induction; the vimentin expression construct was generously provided by Roy Quinlan (University of Durham, Durham, UK). Mutants were created with a Stratagene QuikChange kit and verified by DNA sequencing. Inclusion bodies were purified from bacteria using lysozyme/DNase (30) and were subject to high and low salt washes. Purified inclusion bodies were dissolved in 8 M urea and chromatographed over a SuperDex gel filtration column using a fast protein liquid chromatography system (Amersham Biosciences); fractions were analyzed by SDS-PAGE, and peak fractions were pooled. Purified proteins were incubated in 100 micromolar TCEP (tris-(2-carboxyethyl)phosphine, hydrochloride; Molecular Probes, Eugene, OR) followed by spin labeling with 500 micromolar O-87500 ((1-oxyl-2,2,5,5-tetramethyl- Δ 3-pyrroline-3-methyl) methanethiosulfonate-d15[MTSL-d15]; Toronto Research Chemicals, Toronto, Canada). The spin-labeled protein was separated from unincorporated label by chromatography over a CM-Sepharose column. All purified proteins were stored at -80°C . Filaments were assembled either by dialysis of labeled proteins in a stepwise fashion (31) and aliquots removed at different stages for EPR analysis or by single step dialysis overnight (32). EPR measurements were carried out in a JEOL X-band spectrometer fitted with a loop-gap resonator (33). An aliquot of purified, spin-labeled protein (5 μl) at a final concentration of approximately 100 μM protein was placed in a sealed quartz capillary contained in the resonator. Spectra of samples at room temperature ($20\text{--}22^{\circ}\text{C}$) were obtained by a single 60-s scan over 100 G at a microwave power of 2 milliwatts and a modulation amplitude optimized to the natural line width of 1 G, as described previously (34). Electron microscopy was performed as described by Quinlan and co-workers (31).

RESULTS

Structural Differences between the Central Rod and Carboxyl Tail Domains Revealed by EPR Spectra—Fig. 1 shows the hypothesized domain structure of vimentin and the region studied. Initial experiments were performed to compare the spectra of samples labeled within the central rod or carboxyl terminal tail domains followed by assembly into filaments. Consistent with current models, EPR spectra recorded from mutant vimentin labeled either within the central rod domain at position 316 (Cys³¹⁶) or the tail domain at position 459 (Cys⁴⁵⁹) reveal striking differences in the local structure of these distinct domains (Fig. 2). When unfolded in 8 M urea, the spectra from mutant Cys³¹⁶ and Cys⁴⁵⁹ proteins are identical, with sharp narrow peaks (Fig. 2, green spectra). Upon reduc-

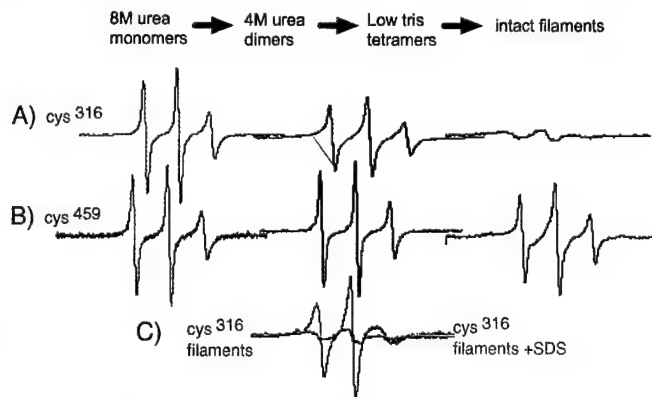


FIG. 2. EPR analysis of assembly. *In vitro* assembly of intermediate filaments occurs through various intermediates, starting with soluble monomers denatured in 8 M urea. EPR spectra can be recorded at any stage; shown are spectra recorded from samples in 8 M urea (green, left), 4 M urea (blue, middle), and assembled filaments (black, right). EPR spectra were recorded from vimentin samples spin-labeled within the central rod (Cys³¹⁶, Ser³²⁸) (A) or near the end of the tail (Ser³²⁸, Cys⁴⁵⁹) (B). C shows the effect of SDS on the intermediate filament structure as reported by position 316. Each spectrum represents the identical number of spins from the same sample, pre- and post-SDS treatment. Interaction between spins in assembled filaments results in a spectrum that is nearly flat (black line). Addition of SDS destroys the IF structure and results in the spectrum with sharp peaks (red line).

tion of urea concentration from 8 to 4 M, corresponding to the assembly of dimers, the spectrum of the label attached to the central rod domain (Cys³¹⁶) becomes more anisotropic, reflecting the adoption of a more ordered structure (Fig. 2A, blue trace) (24, 35). In the assembled filament, the motional freedom of the Cys³¹⁶ side chain is greatly reduced, as revealed by its highly anisotropic spectrum (Fig. 2A, black trace).

In contrast, the spectra from vimentin labeled at Cys⁴⁵⁹ in the tail domain reveals a location that retains a high level of mobility, even in the assembled IF (Fig. 2B, black trace). The sharp peaks of the spectra clearly demonstrate a high level of spin label mobility, indicating a lack of rigid structure. Thus, these two distinct spin-labeled vimentin samples demonstrate that the EPR line shapes can 1) resolve distinct dynamic states associated with specific stages of the assembly process and 2) identify secondary structural features unique to specific IF domains.

The severe broadening of the Cys³¹⁶ intact filament spectra shown in Fig. 2A suggests a magnetic interaction between probes within the assembled filament. Fig. 2C demonstrates how a substantial interaction between labels can be readily identified. The black line displays the EPR spectrum of intact filaments spin-labeled at position 316. The spectrum of the same sample was then collected following addition of SDS (red trace), which disrupts the assembled filament into detergent-solubilized subunits. The large differences in the spectra, where the protein concentration is identical, reveals the extent of interaction between labels. Integration of the SDS-treated sample provides an accurate measure of the total number of spin labels present in the sample. This value can then be used to normalize the intensities between samples according to the total number of spins determined in the presence of SDS.

Analysis of the Amino Terminus of Rod 2B—To test the hypothesis that the initial stage of vimentin assembly is a coiled-coil dimer and to establish whether this dimer was arranged in- or anti-parallel, in-register, or out of register, we engineered a series of single-cysteine mutants at each position from 323 to 336 (as shown in Fig. 1). This sequence spans two contiguous heptad repeats in a region predicted to be rod do-

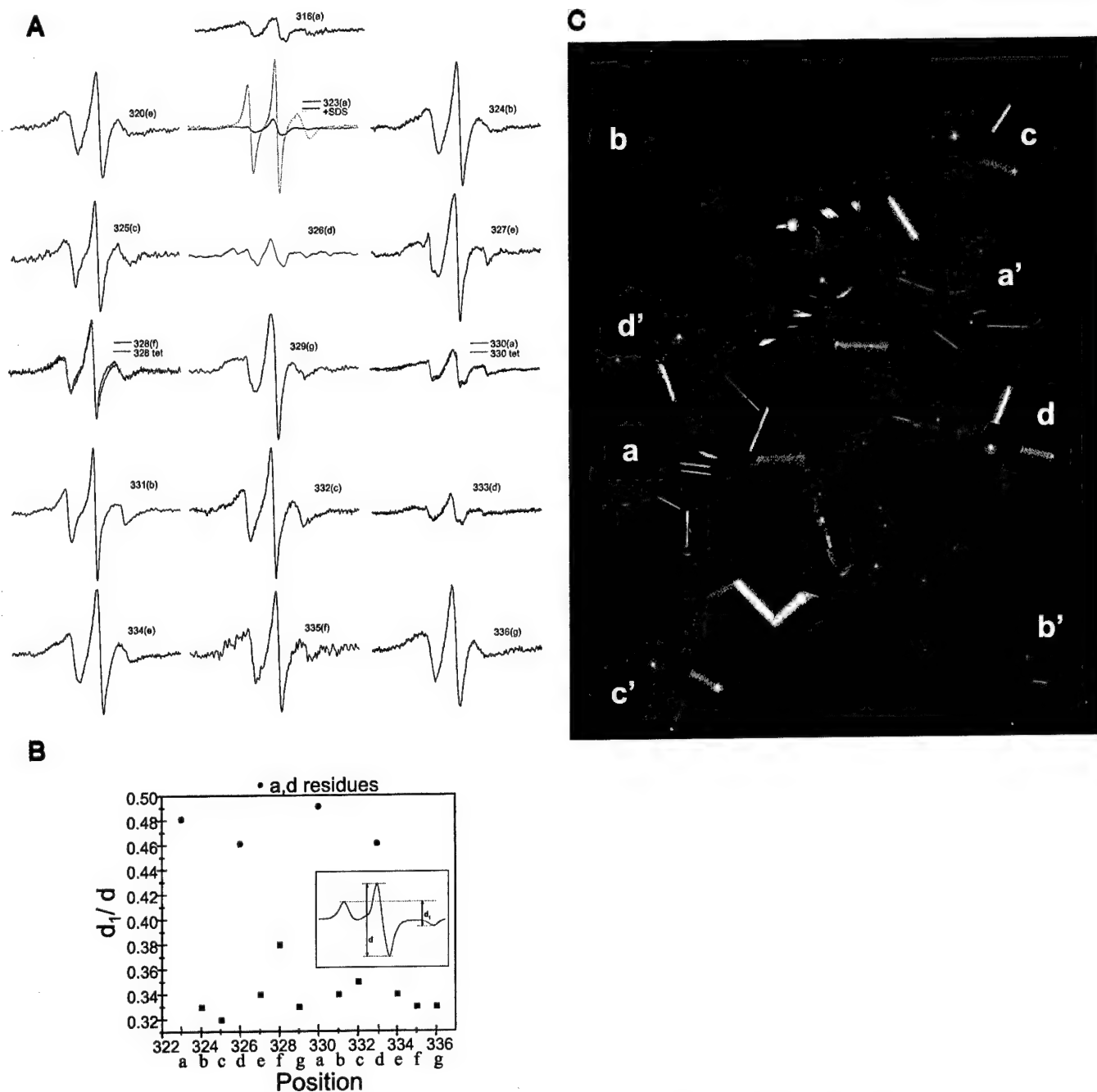


FIG. 3. EPR characterization over two heptad repeats for vimentin spin-labeled at positions 323-336. *A*, room temperature EPR spectra were recorded from assembled intermediate filaments from the indicated mutants. Letters in parenthesis indicate the position of the residue within the heptad repeat. Spectra are scaled according to the same number of spins. The total spins for each sample was determined by adding SDS (final of 2%) to each intermediate filament sample (see position 323, red line) and calculating the double integral, which was then normalized among all samples. The green spectra at positions 328 and 330 represent the normalized spectra for the mutants assembled under low ionic strength conditions that halt assembly at the tetrameric protofilament. *B*, spectral broadening in the absence of motion plotted over positions 323-336. The line-width ratio d_t/d (inset) from spectra acquired at $-100\text{ }^{\circ}\text{C}$ reflects the dipolar interaction strength with a $1/r^3$ dependence (38). *C*, cross-section of a coiled-coil backbone showing the projections of spin-labeled cysteine side chains at the *a* position (red), *b* position (green), *c* position (yellow), and *d* position (purple). The model was constructed with Insight II molecular modeling software (MSI, Inc.) with the solved crystal structure of a 100-amino acid region of cortexillin as the starting template.

main 2B (11, 14, 16). Each mutant contained a single introduced cysteine residue with the wild type cysteine replaced by serine. Mutant proteins were produced by bacterial expression, solubilized in urea, purified, and then spin-labeled. Filament assembly was performed either by single step dialysis overnight (32) or multistep dialysis over several days (31). Assembly into native-looking filaments was confirmed by electron microscopy (31).

Fig. 3A shows the EPR spectra generated from these mutants. The spectrum from each of these mutants, normalized for the same number of spins, reveals that the spin label is in a non-random environment, indicative of a stable backbone and varying degrees of tertiary contact (36). Direct evidence of the coiled-coil structure of the rod domain is provided by the magnetic interactions between labels in close proximity, manifested by increased broadening (most easily seen as a loss in ampli-

tude) of the spectrum when the label is placed in *a* or *d* positions (323, 326, 330, and 333) of the heptad repeat. Thus, these data identify residues that were predicted to appose one another in a coiled-coil configuration.

Evaluation of the broadening as a function of only the distance-dependent dipolar interaction was performed by collecting the EPR spectra of frozen samples. In the absence of motion (*i.e.* frozen in liquid N₂), semi-quantitative analysis of the extent of broadening caused by dipolar interaction can be obtained from the d₁/d spectral ratio (see Fig. 3B, *inset*) (37, 38). Fig. 3B shows the dipolar broadening ratio *versus* sequence position. The difference between *a,d* positions and non-*a,d* positions is demonstrated as a binary distribution of points. The d₁/d ratio for *a,d* positions clusters near 0.5, and the d₁/d ratio for non-*a,d* positions all approach 0.33. These values translate into distances of 1.0 to 1.5 nm for *a,d* positions and >2 nm for all other positions. This analysis provides a measure of the separation between spin labels, revealing the periodicity of the distance separation along the positions of the heptad. From the data, we conclude that these two heptads are assembled in a coiled-coil dimer and that the individual monomers of this dimer are arranged in parallel and in exact register.

To illustrate the α -helical coiled-coil structure within this region of vimentin, we used the recently determined crystal structure of a 100-amino acid region of cortexillin (39) as a model. With this crystal structure as a template for vimentin amino acids 305–405, we used molecular modeling software to introduce spin-labeled cysteine amino acids to heptad positions *a* through *g*. Fig. 3C shows an end-on view of the coiled coil with the spin-labeled side chain of each amino acid position in a different color. The appropriate positions of one heptad are labeled *a-d*, and equivalent positions on the second protein are labeled *a'-d'*. Looking down the helix, positions *a-d* (and *a'-d'*) are labeled red, green, yellow, and purple, respectively. The red and purple moieties are more centrally located, whereas the yellow and green moieties occupy more exterior positions. Spin labels at *a* and *d* positions are close enough to interact within one dimer; positions *b* and *c* are farther separated and at the limit of spin-spin interaction detection. From this modeling and our EPR data of Fig. 3, A and B, the periodicity of the spectra is easily seen to coincide exactly with the helical nature of the coiled coil. Positions *e*, *f*, and *g* of the heptad can also be modeled and reveal the same exterior positions as positions *b* and *c*.

In summary, our examination of vimentin structure within the 323–336 span confirms a self-interaction between labels attached at either the *a* or *d* position. If the monomers were aligned in an anti-parallel manner, then at best, only one residue within the entire rod domain would have shown interaction. Had the monomers been in-parallel, but out of register, then no interaction would have been seen. Thus, SDS-EPR is able to provide the first real-time data that IF monomers are aligned as in-parallel and in-register dimers, within native filaments, formed in physiologic conditions in a manner consistent with predictions of coiled-coil assembly.

Determination of the Structure of Positions 305–316—Having established the ability to identify coiled-coil structures at the level of individual amino acids, we sought to clarify the structure of vimentin positions 305–315, which have been assigned alternately to rod domain 2B or linker 2 (11, 14, 16). Within this sequence, amino acids 305, 309, and 312 were individually changed to cysteine, and the resulting proteins were subject to EPR analysis. As shown in the spectra of these positions (Fig. 4) 305, 309, and 312 resemble the *a-d* positions in line shape and extensive broadening. From these data, we conclude that the vimentin region 305–316 is in an α -helical

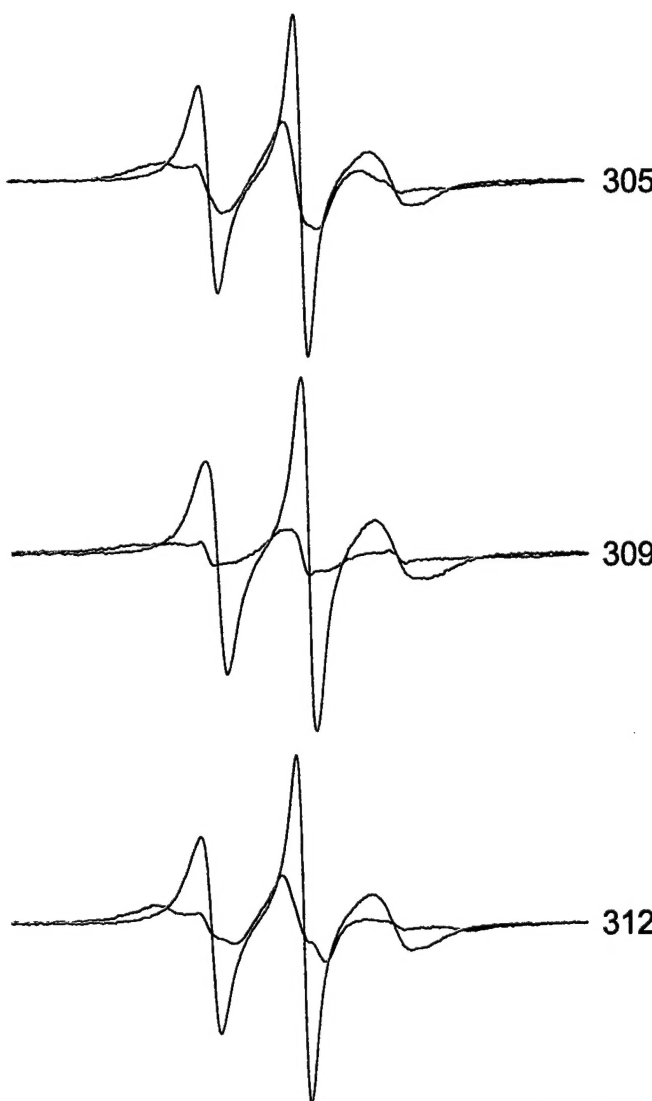


FIG. 4. Room temperature EPR spectra from mutants 305, 309, and 312. Spectra were collected from samples of intact filaments (black) and from SDS-treated filaments (red) at room temperature and normalized as described in the legend to Fig. 2A.

coiled structure, revealing a heptad repeat pattern continuous with the region 323–336 discussed above. Thus, EPR analysis shows that rod domain 2B extends from at least position 305.

Use of EPR to Identify Inter-dimer Interactions—In the previous experiments, *a,d* residues were found to interact because they are positioned at apposing surfaces of two monomers. The lack of interaction of the non-*a-d* residues results from the greater separation between spin labels located on opposite sides of the exterior surface of the dimer. We hypothesized that spin labels such as these, on the surface of the dimer, would permit us to study the precise arrangement of dimers in native filaments. Therefore, we spin-labeled vimentin at multiple positions along the outer surface of the α -helix of the rod domain, assembled filaments, and recorded spectra, looking for evidence of spin label interaction. We found that EPR spectra from spin labels placed at positions 345, 348, and 349 showed evidence of interaction indicating physical proximity. Of these three positions, 348 provided strongest interaction, establishing this residue as a point of overlap between two dimers (Fig. 5A).

Interaction between spin labels at position 348 is interpreted as resulting from an interaction between spin labels attached to separate dimers. Support for this conclusion is provided by

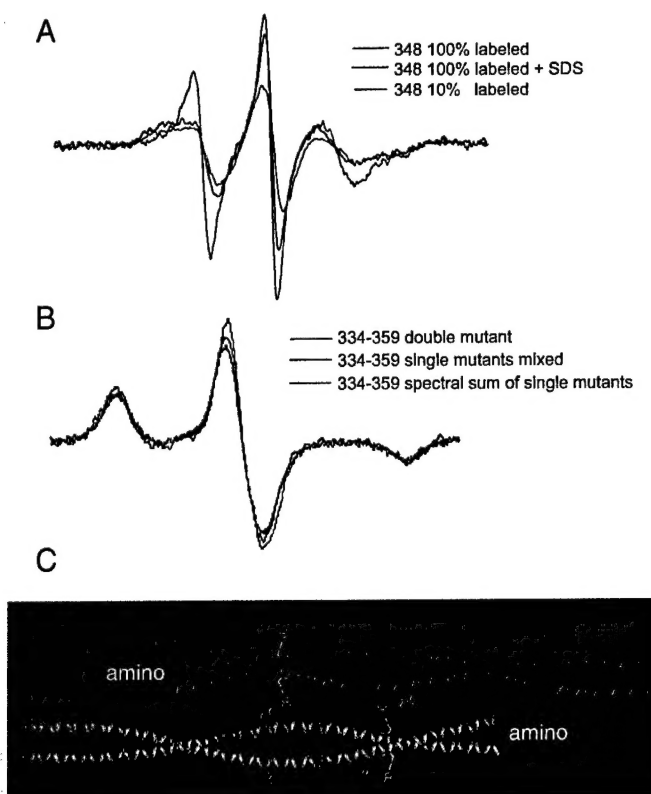


FIG. 5. Alignment of vimentin dimers detected by spin interaction. *A*, room temperature EPR spectra from filaments containing 100 and 10% labeled Cys³⁴⁸ vimentin. All three spectra reflect the same number of spins. Scaling was accomplished by the addition of 2% SDS to the 10 and 100% samples and by normalizing the resulting double integrals. The 100% labeled sample is clearly more broadened (black line) than the 10% labeled sample (blue line). The sample with 10% labeled Cys³⁴⁸ was prepared from a mixture of unlabeled wild type vimentin and 100% labeled Cys³⁴⁸ vimentin (9:1). *B*, the dipolar interaction between labels attached at positions 334 and 359 observed in the EPR spectra of frozen filaments. The 334–359 double mutant (black line) contains the two Cys substitutions within the same gene. The 334 + 359 mixture (red line) contains equal amounts spin-labeled Cys³³⁴ and Cys³⁵⁹ vimentin, which were prepared by isolating and spin labeling each protein separately. For experiments in *A* and *B*, protein concentrations were measured using a Pierce BCA assay kit, with bovine serum albumin as a standard. Appropriate amounts of protein were then mixed, and filament assembly was performed using a single step dialysis procedure. The amount of dipolar broadening relative to the spectral sum of single labeled 334 + single labeled 359 (green) was analyzed using a Pake deconvolution of normalized spectra (see “Results”). The three scans normalized to the same number of spins were obtained over 200 G at –100 °C (although only a 100 G portion is shown). *C*, ribbon diagram of an α -helical coiled coil indicating the locations of 334 (yellow), 348 (red), and 359 (blue) on the outside of the helices. Shown are spin-labeled Cys substitutions along the coiled-coil backbone structure obtained from the x-ray crystal structure of a 100-amino acid cortexillin fragment (39), which exists as an α -helical coiled coil. The molecular model was constructed using Insight II software.

comparing EPR spectra from samples with different proportions of spin label (25). A sample of vimentin containing 10% spin-labeled 348 and 90% wild type vimentin produces a spectrum that shows no evidence of spin-spin interaction; the spin labels are diluted and very rarely interact. The traces in Fig. 5*A* each represent the same number of spins as determined from the integration of the sample following addition of SDS. The spectrum from protein completely labeled at position 348 (100%, Fig. 5*A*, black line) is significantly more broadened than from the sample containing 10% labeled 348 (Fig. 5*A*, blue line). The spectrum of the 10% sample demonstrates that position 348 is a non- α, δ residue of the heptad (compare the spectra to those in Fig. 3*A*), but the spectrum from the 100% labeled

sample is broadened. Note that each dimer contains two spin-labeled positions, but only one would be predicted to interact with the second dimer. The second spin-labeled position of each dimer is on the opposite side and would be predicted not to interact unless tetramers assemble further.

Although the data in Fig. 5*A* show that position 348 is a site of interaction between dimers, these data do not identify whether these dimers are arranged in- or anti-parallel. Unambiguous demonstration of the anti-parallel alignment of dimers with a midpoint overlap at position 348 is provided by EPR spectra of mixtures of spin-labeled proteins (Fig. 5*B*). We selected position 334 as the starting point on the outside of the helix (an ϵ position) and predicted that a site within the region of 355–365 would interact with 334 if dimers were arranged in an anti-parallel fashion. Therefore, mutants at positions 356(b heptad position), 359(e), 363(b), or 366(e) on the outside of the helix were prepared. Spin-labeled 334 was individually mixed equimolar with each spin-labeled 356, 359, 363, or 366 mutant. Assembly of each mixture into filaments was confirmed by electron microscopy, and EPR spectra were collected. To evaluate these combinations independently of line shape differences arising from differences in the rate of rotational averaging of hyperfine anisotropy, EPR analysis was performed on the samples frozen at –100 °C. Quantitative analysis of the spectra was achieved using a Pake deconvolution of broadening functions (40, 41), which optimizes results according to both the strength of the interaction and the fraction of interacting species. Only the mixture of the 334 and 359 spin-labeled proteins displayed evidence of interaction as seen by significant broadening of the spectra (Fig. 5*B*). From this mixture, the Pake deconvolution optimization of frozen spectra resulted in a mean interspin distance of 1.6 nm, with a non-interacting fraction of 74%. This labeling level coincides with a distribution of approximately one quarter of the spins interacting. Given an equal number of labeled 334 and 359 proteins introduced into the assembly mixture and a random pairing of these proteins during assembly, the expected population of spins paired at the tetramer level is 25%. Thus, these results provide strong evidence that vimentin dimers in intact filaments are associated in an anti-parallel manner, overlapping within 1.6 nm of position 348.

In observing the interaction between positions 334 and 359, more broadening would be predicted if spin labels were placed at both 334 and 359 within the same polypeptide chain. Hence we constructed a double mutant that codes for a Cys substitution at both position 334 and position 359. To simplify analysis, the assembly of the 334–359 double mutant was performed in low ionic strength Tris buffer; under these conditions, tetrameric protofilaments have been demonstrated to predominate (22, 42, 43). EPR spectra of the 334–359 double mutant (Fig. 5*B*, black line) is different from the spectral sum of the individual mutants (green line). A Pake deconvolution analysis of the double mutant collected at –100 °C was optimized with a mean interaction distance of 1.7 nm and a non-interacting population of 57%. The results correspond to a system in which approximately half of the spins are interacting, matching the alignment predicted by the experiments using a mixture of single-labeled proteins. Thus, EPR spectra provide evidence for the interaction of positions 334 and 359 within vimentin tetramers. Furthermore, quantitative analysis supports the hypothesis that vimentin in low ionic strength Tris is a relatively homogeneous population of tetramers arranged anti-parallel with rod 2B interacting.

Visualization of the side chain interactions identified between position 348 and itself, as well as 334 and 359, is provided in Fig. 5*C*. As in Fig. 2*C*, we have used the crystal structure of cortexillin as a model for vimentin dimer structure

and have arranged two dimers in a structure consistent with our EPR data. Within the figure, the spin-labeled side chain of position 334 is shown in *yellow*; 348 is *red*, and 359 is *blue*. No other side chains are shown. As depicted, interactions between 348 and 348 as well as 334 and 359 can be seen.

DISCUSSION

The data presented conclusively show that assembly of vimentin intermediate filaments can be studied by site-directed spin labeling and EPR. In summary, our examination of vimentin structure within the 323–336 span confirms a self-interaction between labels attached at either the *a* or *d* position. If the monomers were aligned in an anti-parallel manner, then at best, only one residue within the entire rod domain would have shown interaction. Had the monomers been in parallel but out of register, then no interaction would have been seen. Spectral data provide precise structural information detailing the protein–protein contacts between IF proteins in intact filaments. Thus, SDSL-EPR is able to provide the first real-time data that IF monomers are aligned as in-parallel and in-register dimers, within native filaments formed in physiologic conditions in a manner consistent with predictions of coiled-coil assembly.

Our data reveal the α -helical coiled-coil nature of the vimentin rod domain and provide evidence that the region 305–336 is an α -helical coiled coil; this identification resolves a discrepancy in the literature (11, 14).

Two factors account for the broad spectra reported by the *a,d* positions. First, the wide splittings reflect a lack of motional averaging by side chains located at these positions. This indicates that the rotational freedom of the label is restricted by the protein structure. Second, the magnitude of broadening suggests a dipolar interaction among the labels when they are attached at either an *a* or *d* position. Thus the dynamic and spatial observations of spin-labeled positions within this span provide the first direct evidence of an α -helical coiled-coil arrangement with an exact register of the two peptide chains. Non-*a,d* positions, predicted to be on the exterior of the dimer, do not reveal such strong broadening, indicating that spin labels are farther apart, yet the overall structure is ordered and α -helical.

Beyond determination of structure, we have used SDSL-EPR to study assembly of IFs. We have been able to collect spectra from samples in low ionic strength Tris and subsequently from the same samples assembled into filaments. A surprising finding was that little change in rod domain structure is observed between normalized spectra obtained from fully assembled filaments and protofilaments formed in low ionic strength Tris. Under these conditions, higher order assembly beyond tetrameric protofilaments is inhibited, resulting in a predominantly tetramer population (22, 42, 43). Two examples of tetramer spectra are shown in Fig. 3A (*green line*). This suggests that vimentin assembly beyond the tetramer level does not generate strong tertiary contacts involving the rod domain examined here. Thus, we do not see evidence for a tight packing of neighboring tetramers via their rod domains. This is consistent with the fact that non-*a,d* positions display moderate motional freedom even in the intact filament.

As shown in Fig. 3C, non-*a,d* positions are widely separated on the outside of the helix. In a fortunate coincidence, this degree of separation is just slightly greater than the distance EPR can be used to measure. Thus, we have used spin labels placed on the outside of the helix to study interactions between dimers in filaments and assembly intermediates. With this strategy, we have identified an anti-parallel arrangement of dimers that is one of the configurations suggested by Steinert *et al.* from protein cross-link data (20). Our conclusions extend the data of Steinert *et al.* (20) and identify amino acid position

348 as the midpoint of overlap. Additionally, we have predicted an interaction between adjacent dimers and identified an interaction between positions 334 and 359 of adjacent dimers; this interaction thus proves the ability of EPR to identify interaction between the outer surfaces of two adjacent α -helices. This identification allows for the rational prediction of amino acids that interact between adjacent rods 2B in the anti-parallel arrangement.

Our data validate our experimental approach and provide a method for understanding the individual mechanisms behind the growing number of IF gene mutations identified as causing inherited genetic diseases. Because of the numbers and locations of identified mutations, each is likely to have subtle differences from the others. Abnormal assembly products can now be characterized by EPR at any stage during assembly, and the mechanisms behind such abnormal assembly can be elucidated. More broadly, these data establish the utility of SDSL-EPR to provide structural data on filament-forming proteins in general.

Acknowledgment—We thank Dr. Christian Altenbach for kindly providing the Pake deconvolution and simulation program.

REFERENCES

1. Lane, E. B., Rugg, E. L., Navsaria, H., Leigh, I. M., Heagerty, A. H., Ishida-Yamamoto, A., and Eady, R. A. (1992) *Nature* **356**, 244–246
2. Irvine, A. D., Corden, L. D., Swensson, O., Swensson, B., Moore, J. E., Frazer, D. G., Smith, F. J., Knowlton, R. G., Christophers, E., Rochels, R., Uitto, J., and McLean, W. H. (1997) *Nat. Genet.* **16**, 184–187
3. Brenner, M., Johnson, A. B., Boesplug-Tanguy, O., Rodriguez, D., Goldman, J. E., and Messing, A. (2001) *Nat. Gen.* **27**, 117–120
4. Bonifas, J. M., Rothman, A. L., and Epstein, E. H., Jr. (1991) *Science* **254**, 1202–1205
5. Coulombe, P. A., Hutton, M. E., Letai, A., Hebert, A., Paller, A. S., and Fuchs, E. (1991) *Cell* **66**, 1301–1311
6. Fuchs, E., and Cleveland, D. W. (1998) *Science* **279**, 514–519
7. Herrmann, H., Strelkov, S. V., Feja, B., Rogers, K. R., Brettel, M., Lustig, A., Häner, M., Parry, D. A., Steinert, P. M., Burkhardt, P., and Aeby, U. (2000) *J. Mol. Biol.* **298**, 817–832
8. Strelkov, S. V., Herrmann, H., Geisler, N., Lustig, A., Ivaninskii, S., Zimbelmann, R., Burkhardt, P., and Aeby, U. (2001) *J. Mol. Biol.* **306**, 773–781
9. Hanukoglu, I., and Fuchs, E. (1983) *Cell* **33**, 915–924
10. Steinert, P. M., Steven, A. C., and Roop, D. R. (1985) *Cell* **42**, 411–420
11. Albers, K., and Fuchs, E. (1992) *Int. Rev. Cytol.* **134**, 243–279
12. Bader, B. L., Magin, T. M., Hatzfeld, M., and Franke, W. W. (1986) *Embo J.* **5**, 1865–1875
13. Hess, J. F., Casselman, J. T., and FitzGerald, P. G. (1993) *Curr. Eye Res.* **12**, 77–88
14. Conway, J. F., and Parry, D. A. D. (1988) *Int. J. Biol. Macromol.* **10**, 79–98
15. Steinert, P. M., and Roop, D. R. (1988) *Annu. Rev. Biochem.* **57**, 593–625
16. Fuchs, E., and Weber, K. (1994) *Annu. Rev. Biochem.* **63**, 345–382
17. Crick, F. H. C. (1953) *Acta Crystallogr.* **6**, 689–697
18. Cohen, C., and Parry, D. A. D. (1986) *Trends Biol. Sci.* **11**, 245–248
19. Steinert, P. M., Marekov, L. N., Fraser, R. D., and Parry, D. A. (1993) *J. Mol. Biol.* **230**, 436–452
20. Steinert, P. M., Marekov, L. N., and Parry, D. A. (1993) *J. Biol. Chem.* **268**, 24916–24925
21. Quinlan, R. A., Hatzfeld, M., Franke, W. W., Lustig, A., Schulthess, T., and Engel, J. (1986) *J. Mol. Biol.* **192**, 337–349
22. Rogers, K. R., Herrmann, H., and Franke, W. W. (1996) *J. Struct. Biol.* **117**, 55–69
23. Perozo, E., Cortes, D. M., and Cuello, L. G. (1999) *Science* **285**, 73–78
24. Hubbell, W. L., Cafiso, D. S., and Altenbach, C. (2000) *Nat. Struct. Biol.* **7**, 735–739
25. Langen, R., Isas, J. M., Luecke, H., Haigler, H. T., and Hubbell, W. L. (1998) *J. Biol. Chem.* **273**, 22453–22457
26. Sandilands, A., Masaki, S., and Quinlan, R. A. (1998) in *Intermediate Filaments Subcellular Biochemistry* (Herrmann, H., and Harris, J. R., eds) Vol. 31, pp. 291–318, Plenum Press, New York
27. Colucci-Guyon, E., Portier, M. M., Dunia, I., Paulin, D., Pournin, S., and Babinet, C. (1994) *Cell* **79**, 679–694
28. Conley, Y. P., Erturk, D., Keverline, A., Mah, T. S., Keravala, A., Barnes, L. R., Bruchis, A., Hess, J. F., FitzGerald, P. G., Weeks, D. E., Ferrell, R. E., and Gorin, M. B. (2000) *Am. J. Hum. Genet.* **66**, 1426–1431
29. Jakobs, P. M., Hess, J. F., FitzGerald, P. G., Kramer, P., Weleber, R. G., and Litt, M. (2000) *Am. J. Hum. Genet.* **66**, 1432–1436
30. Nagai, K., and Thøgersen, H. C. (1987) *Methods Enzymol.* **153**, 461–481
31. Carter, J. M., Hutcheson, A. M., and Quinlan, R. A. (1995) *Exp. Eye Res.* **60**, 181–192
32. Herrmann, H., Hofmann, I., and Franke, W. W. (1992) *J. Mol. Biol.* **223**, 637–650
33. Hubbell, W. L., Froncisz, W., and Hyde, J. S. (1987) *Rev. Sci. Instrum.* **58**, 1879–1886
34. Chomiki, N., Voss, J. C., and Warden, C. H. (2001) *Eur. J. Biochem.* **268**,

903–913

35. Hubbell, W. L., Gross, A., Langen, R., and Lietzow, M. A. (1998) *Curr. Opin. Struct. Biol.* **8**, 649–656
36. Mchaourab, H., Lietzow, M. A., Hideg, K., and Hubbell, W. L. (1996) *Biochemistry* **35**, 7692–7704
37. Kokorin, A. I., Zamaraev, K. I., Grigorian, G. L., Ivanov, V. P., and Rozantsev, E. G. (1972) *Biofizika* **17**, 34–41
38. Likhtenshtein, G. I. (1993) *Biophysical Labeling Methods in Molecular Biology*, pp. 57–62, Cambridge University Press, New York
39. Burkhard, P., Kammerer, R. A., Steinmetz, M. O., Bourenkov, G. P., and Aeby, U. (2000) *Structure Fold. Des.* **8**, 223–230
40. Rabenstein, M. S., and Shin, Y.-K. (1995) *Proc. Natl. Acad. Sci. U. S. A.* **92**, 8239–8243
41. Altenbach, C., Oh, K.-J., Trabanino, R. E., Hideg, K., and Hubbell, W. L. (2001) *Biochemistry* **40**, 15471–15482
42. Meng, J. J., Khan, S., and Ip, W. (1994) *J. Biol. Chem.* **269**, 18679–18685
43. Potschka, M., Nave, R., Weber, K., and Geisler, N. (1990) *Eur. J. Biochem.* **190**, 503–508